Ni and CO Used as Probes of the Amorphous Silica Surface: IR and Theoretical Studies of Dicarbonyl Ni^{II} Complexes†

Gianmario Martra,[||,‡] Salvatore Coluccia,[§] Michel Che,[||,#] Laurent Manceron,[⊥] Maggy Kermarec,[||] and Dominique Costa*[,||]

Laboratoire de Réactivité de Surface, UMR 7609, CNRS, Université Pierre et Marie Curie, 4 place Jussieu, 75252 Paris Cedex 05, France, Dipartimento di Chimica IFM, Università di Torino, Via P. Giuria 7, 10125 Torino, Italy, and LADIR-Spectrochimie moléculaire, UMR 7075, CNRS, Université Pierre et Marie Curie, 75252 Paris Cedex 05, France

Received: March 28, 2003; In Final Form: April 17, 2003

This paper is the continuation of a study of $Ni^{II}-(CO)_n$ complexes formed on amorphous silica. Both Ni and CO are used as successive probes of the local structure and reactivity of the silica surface. An isolated tricoordinated Ni^{II}_{3c} ion in a single oxidation state is characterized with CO as a probe of the coordination vacancies of the transition metal. An experimental FTIR study shows two main types of Ni^{II} dicarbonyl with equivalent and nonequivalent COs formed from the Ni^{II} monocarbonyl previously characterized in *J. Am. Chem. Soc*. **2002**, *24,* 7210−7217, whereas no tricarbonyl Ni^{II} complex is observed. Theoretical models are tested using experimental CO frequencies: DFT calculations with the cluster approach already used for the Ni^{II} monocarbonyl complex allow us to gain valuable information on the local environment of the Ni^{II} ion. For Ni^{II} dicarbonyls, information can be obtained on the second coordination sphere of Ni^{II} (namely, Si atoms) whereas for monocarbonyls, only first oxygen neighbors were concerned. Then, by embedding the small silica fragments in silica rings really existing on the surface, we can bridge the "reality gap" between the theoretical model and its application to IR studies. We show that the Ni^{II}_{3c} ion is stabilized by an 8T or 9T ring with an adjacent strained 2T ring (where *n*T represents the number of silicon atoms in a ring).

Introduction

Recent reports attest the importance of CO as a molecular probe to investigate the morphology of oxide supports.[1,2] The interest in CO is related to its ability to interact with oxide surfaces by either C or O or by both. CO can bind to a transition metal (TM) ion of various oxidation states by the carbon atom, whereas the oxygen atom can either bridge an adjacent TM or be hydrogen-bonded to OH groups of the support testing thus the acidic properties of the material.[3] Thus, CO can be used to probe the oxidation state and the interfacial coordination chemistry of TMs grafted onto oxide surfaces by filling the coordination vacancies. Moreover, it can form organometallic complexes with metal−carbon bonds allowing us to bridge the gap between organic and coordination chemistries.[4]

Upon CO adsorption, supported TM ions in low oxidation states (0 or 1) are known to give rise to mono- and polycarbonyl complexes with easy substitution of O-terminated surface groups acting as ligands with CO.[5−8] However, for higher oxidation states, mono- and dicarbonyl complexes are still observed but the interconversion between carbonyl species and surface ligands of the support is less likely, probably because of the stronger electrostatic interaction between the metal ion and the oxygen anions. This is the case for the Mo^{V}/SiO_2 and Mo^{IV}/SiO_2 (or Al_2O_3) systems for which dicarbonyl complexes were characterized.[9,10] $[Ru(CO)_n]^{\delta+}$ complexes with $n = 2$ or 3 and $\delta = 1-3$ have also been identified.[11−19]

For silica-supported Ni catalysts, our initial interest was to characterize by electron paramagnetic resonance (EPR) Ni^{I} ions known to be active in olefin oligomerization.[20] Because not all Ni^{II} ions were reduced to Ni^{I} ions, the characterization of the Ni^{II}/SiO_2 precursor system was also performed. In a previous work on silica-supported Ni catalysts, Rebenstorf and Larsson reported on the identification of carbonyl Ni^{II} complexes by IR.[21] However, the adsorption of CO at 293 K gave rise to reduced species such as Ni^{I} and Ni^{0} leading to a speculative assignment of the various carbonyl species.

In previous work,[22a] TM was first used to probe the adsorption sites on the silica surface. It was shown that Ni^{II} ions could be grafted to silica in an isolated manner and were tricoordinated to silica, noted as Ni^{II}_{3c}, providing a suitable activating treatment at 973 K had been performed.[22a] Then, DFT calculations based on a cluster approach[22b] showed that the $[Si_5O_8H_2-Ni^{II}]$ cluster satisfactorily reproduced the experimental diffuse reflectance spectroscopy (DRS) and extended x-ray absorption fine structure EXAFS data, that is, the Ni^{II} 3-fold coordination and the NiO distances, respectively.[22a]

The next step was to use CO to probe the coordination vacancies around the TM. In the first part of this work, a single monocarbonyl formed from Ni^{II}_{3c} ions was identified by FTIR spectroscopy upon CO adsorption at pressures <4 Pa[23] and at 77 K, the temperature at which the Ni^{II} oxidation state is retained. The preceding neutral $[Si_5O_8H_2-Ni^{II}]$ cluster failed to reproduce the ν_{CO} frequency of the corresponding mono-

† Dedicated to Professor F. A. Cotton.

* To whom correspondence should be addressed. Tel: 33 01 44 27 60 05. Fax: 33 01 44 27 60 33. E-mail: costa@ccr.jussieu.fr.

|| Laboratoire de Réactivité de Surface, UMR 7609, CNRS, Université Pierre et Marie Curie.

‡ Present address: Dipartimento di Chimica IFM, Università di Torino, Via P. Giuria 7, 10125 Torino, Italy.

Member of the Institut Universitaire de France.

§ Dipartimento di Chimica IFM, Università di Torino.

⊥ LADIR-Spectrochimie moléculaire, UMR 7075, CNRS, Université Pierre et Marie Curie.

10.1021/jp034794q CCC: $25.00
Published on Web 05/29/2003

carbonyl complex, whereas the $[(Si_5O_3)Ni^{II}]^+$ cluster well reproduced the Ni−O distances found by EXAFS and also the experimental ν_{CO} frequency.

The aim of this work is first to test the validity of this charged silica cluster on polycarbonyls formed at higher CO pressure. Dicarbonyl complexes with *equivalent* or *nonequivalent* CO oscillators are characterized by FTIR in the $4 < p_{CO} < 6$ Pa range. Modeling dicarbonyl complexes with equivalent COs by using the above-mentioned $[(Si_5O_3)Ni^{II}]^+$ cluster shows that the CO probe is sensitive to the second coordination sphere, that is, the next-nearest Si neighbors, in contrast to the case of monocarbonyls for which the CO probe is mainly sensitive to the charge of the cluster and to the oxygen neighbors nearest to Ni. A second objective of the modeling study is to represent the surface by rings that really exist on the surface of amorphous silica. The small initial $[(Si_5O_3)Ni^{II}]^+$ cluster is thus embedded in silica rings of increasing size to identify the convenient ring that can accommodate the Ni^{II}_{3c} ion.

The approach followed in this work is the use of the Ni^{II} ion and CO molecule as probes of the local structure and reactivity of the silica surface. The CO probe, through the various carbonyl complexes produced upon its adsorption, gives information on the lability of the oxygens of the support and on the flexibility (or rigidity) of silica. Another important feature of this work is that CO allows us to probe the validity of the theoretical models used to represent silica via the fit between the experimental ν_{CO} frequency and those derived theoretically for each model.

Experimental Section

Two amorphous silica-supported Ni samples (nonporous silica Aerosil A 380 supplied by Degussa, purity >99.5%, S_{BET} = 380 $m^2 \cdot g^{-1}$), referred to as ENi(NH_3) and ENi(en) (Ni = 2 wt %), were prepared by competitive cationic exchange and further activation at 973 K. The procedures of exchange and activation have already been described in the first part of this work.[23] The amine and en ligands are eliminated after activation at 973 K. These samples differ in the dispersion of Ni^{II} ions, ENi(en) containing only isolated Ni^{II}_{3c} ions and ENi(NH_3) containing also a very small amount of next-nearest Ni backscatterers assigned to the presence of small NiO particles.[22a]

The FT-IR spectra were recorded using a Bruker IFS 66V spectrometer using a 4 cm^{-1} resolution and 256 coadded scans. The IR spectra of CO adsorbed at 77 K are reported in absorbance, the spectrum of the activated pellet taken as the background.

Modeling calculations were performed using the Gaussian 94 program.[24] The geometrical parameters of the carbonyl complexes were optimized at the DFT level using the Becke's three-parameter hybrid method with the Lee−Yang−Parr correlation functional (B3LYP)[25] and checked by vibrational analysis. The basis set is a double ζ plus polarization basis (DZVP2).[26] The methodology to optimize the various dicarbonyl complexes is reported in ref 27. The results were not corrected for basis set superposition error (BSSE) or zero-point energy vibrational effects, leading thus to an overestimate of bond strengths. Calculations were performed for the singlet and triplet spin states. The results concerning the carbonyl complexes account for the singlet, which was found to be the most stable state. The calculated frequencies are corrected by a scaling factor taking into account the anharmonicity. This factor, equal to 0.988, is derived from free CO (experimental value of ν_{CO}/calculated value). Because we investigate a dicarbonyl complex with equivalent COs, in a first step the CO and the NiC bond lengths of the two COs are coupled in the geometry optimizations. Then, they are left free to relax. The $[(Si_5O_3)Ni^{II}]^+$ and $[(SiO)(SiOSi)Ni^{II}]^+$ clusters are optimized in the triplet state.[25]

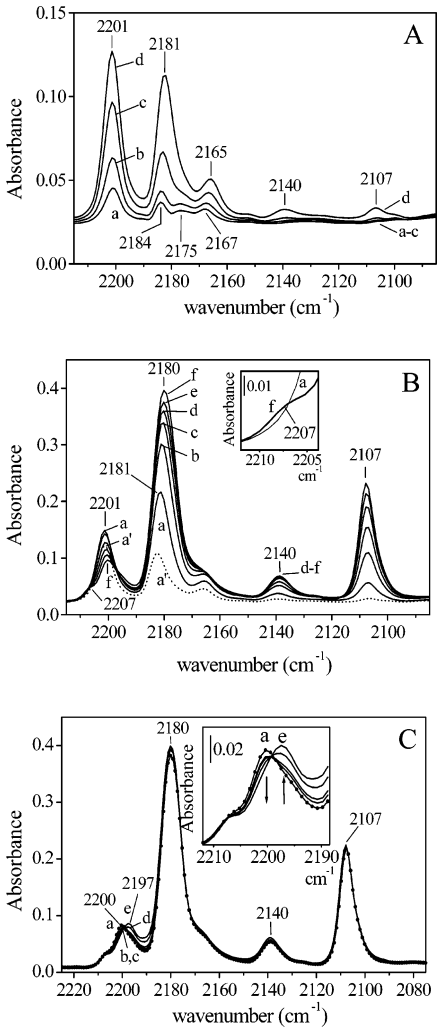

Figure 1. Infrared spectra of ^{12}CO adsorbed at 77 K on ENi(NH_3) under (A) low ^{12}CO pressures [(a) 3×10^{-1}, (b) 6×10^{-1}, (c) 1, and (d) 3.5 Pa], (B) medium ^{12}CO pressures [from (a) 4 to (f) 6 Pa; (a′) dotted line spectrum corresponding to spectrum d in panel A with p_{CO} = 3.5 Pa; (inset) close up view of the 2210−2205 cm^{-1} range], and (C) high ^{12}CO pressures [(a) 6, (b) 10, (c) 20, (d) 45, and (e) 60 Pa; (inset) close up view of the isobestic point].

Results and Discussion

A. Infrared Study. *1. Medium and High CO Coverages.* 1.1. IR Spectra of ^{12}CO Adsorbed on Activated ENi(NH_3). Three domains of CO pressure have been selected (Figure 1A−C). The spectra corresponding to the low CO pressure domain (see part I)[23] are shown for the sake of clarity (Figure 1A). In the second pressure domain, corresponding to $4 < p_{CO} < 6$ Pa, the overall intensity increases significantly (notice the different absorbance scale). It is observed that further increase of the CO pressure causes a progressive depletion of the 2201 cm^{-1} band, whereas the 2181 and 2107 cm^{-1} peaks strongly increase in intensity (Figure 1B, spectra a−f). However, these two components do not grow up in a related way, because their intensity ratio, I_{2180}/I_{2107}, significantly decreases during this process from 6.0 (Figure 1B, spectrum a) to 1.8 (Figure 1B, spectrum f).

The 2181 cm^{-1} peak, which exhibits an asymmetric profile, shifts to 2180 cm^{-1} and becomes broader with its width at half-maximum increasing from 8 (Figure 1B, spectrum a) to 10 cm^{-1} (Figure 1B, spectrum f). Moreover, the depletion and broadening

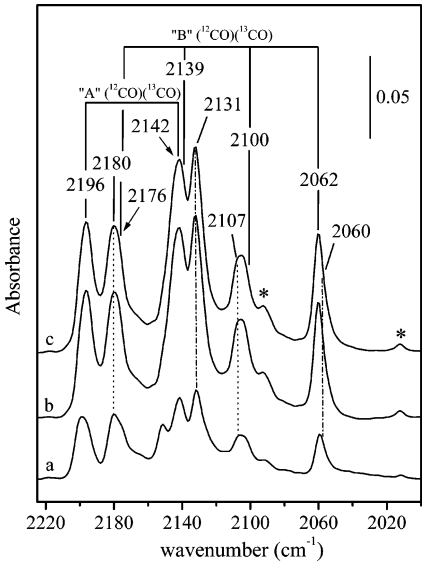

Figure 2. Infrared spectra of a ^{12}CO−^{13}CO (50:50) mixture adsorbed at 77 K on ENi(NH_3) sample under (a) 4, (b) 6, and (c) 60 Pa. Vertical full lines correspond to mixed ^{12}CO−^{13}CO species for A type (equivalent CO) and B type dicarbonyls (nonequivalent CO). Vertical dotted lines and dashed−dotted lines, respectively, correspond to $^{12}(CO)_2$ and to $^{13}(CO)_2$ species for type B dicarbonyls. The ∗ correspond to $^{13}C^{18}O$ species.

of the 2201 cm^{-1} band, which shifts to 2200 cm^{-1}, are accompanied by the progressive appearance of a very weak absorption at 2207 cm^{-1} (Figure 1B, spectra a−f and inset).

In the third domain ($6 < p_{CO} < 60$ Pa) (Figure 1C), the admission of CO causes a further decrease in intensity of the 2200 cm^{-1} component but now in favor of a new absorption growing up at 2197 cm^{-1}, whereas the intensity of the 2180 and 2107 cm^{-1} bands does not significantly change. An isosbestic point at 2199 cm^{-1}, where the decreasing (2200 cm^{-1}) and increasing (2197 cm^{-1}) components cross one another, is observed.

After this transformation, further increase of the CO pressure up to 400 Pa does not affect the bands, only producing absorptions at 2165 and 2136 cm^{-1} (spectra not reported for the sake of brevity). These bands, observed when CO is adsorbed on bare silica, are due to CO interacting with surface hydroxyl groups and to "liquid-like" CO, respectively.[28] These bands completely disappear upon outgassing CO at 77 K and are reversibly restored after a subsequent CO adsorption.

1.2. IR Spectra of ^{12}CO−^{13}CO (50:50) Adsorbed on Activated ENi(NH_3). Several supported transition metal ions are known to form polycarbonyl adducts.[10,21b] The presence of polycarbonyl species is usually investigated by means of the isotopic substitution method, by adsorbing a ^{12}CO−^{13}CO mixture.[29] The ^{12}CO−^{13}CO (50:50) mixture was adsorbed onto the sample with increasing pressures. However, only the spectra recorded for the typical pressure domains previously described (Figure 1B, spectra a and f; Figure 1C, spectrum e) are reported in Figure 2.

Bands at 2196, 2142, and 2062 cm^{-1} and also partially resolved components around 2176 and 2100 cm^{-1} appear in the spectra, in addition to absorptions due to either ^{12}CO or ^{13}CO (Figure 2, spectra a and b). It may be noticed that the band at 2196 cm^{-1} is really different from the weak component observed at 2197 cm^{-1} at higher coverage of pure ^{12}CO (Figure 1C, spectrum e). The 2196 cm^{-1} band shown in Figure 2, spectra b and c, is observed for ^{12}CO−^{13}CO pressures corresponding

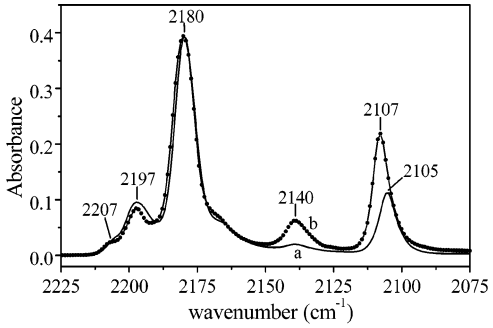

Figure 3. Infrared spectra of ^{12}CO adsorbed at 77 K under a pressure of 60 Pa on (a) ENi(NH_3) and (b) ENi(en).

to the same ^{12}CO pressure range producing the spectra shown in Figure 1B, in which the 2197 cm^{-1} band is completely absent.

1.3. IR Spectra of ^{12}CO Adsorbed on Activated ENi(en). Absorption bands exhibiting almost the same spectral positions and dependence on CO pressure as those described for the ENi(NH_3) system were obtained. However, some relevant differences in their relative intensities with respect to the previous case were observed.

This is shown in Figure 3, in which the spectra of both samples are compared at $p_{CO} = 60$ Pa, the intensities of the reported bands being normalized with respect to the intensity of the 2180 cm^{-1} peak. For the ENi(en) sample (Figure 3a, full line), the 2140 cm^{-1} band is almost absent. Moreover, the low-frequency component observed at 2107 cm^{-1} is strongly reduced in intensity with respect to that observed for the ENi(NH_3) sample (Figure 3b, dotted line) and shifts toward 2105 cm^{-1}. A narrower peak at 2180 cm^{-1} and a broader band at 2197 cm^{-1} are also observed for ENi(en).

2. Attribution of the IR Bands. In part I,[23] the 2201 cm^{-1} band was attributed to the monocarbonyl complex. This component, which initially increases in intensity with CO pressure (Figure 1A), is progressively depleted in favor of the other bands (Figure 1B,C). This behavior suggests that the monocarbonyl species, stable in a very limited CO pressure range, is converted into polycarbonyl adducts upon increasing the CO pressure.[30]

2.1. Bands at 2197, 2180, and 2107 cm^{-1}: Dicarbonyl Ni^{II}_{3c} Species. Growing in intensity at the expense of the monocarbonyl component at 2201 cm^{-1}, the bands at 2180 and 2107 cm^{-1} at low CO pressure (Figure 1B) and the band at 2197 cm^{-1} (Figure 1C) at higher CO pressure can be reasonably assigned to dicarbonyl adducts, as expected from the addition of one CO to the monocarbonyl. However, the different intensity ratios of the 2180 and 2105 cm^{-1} bands for ENi(en) and the 2180 and 2107 cm^{-1} bands for ENi(NH_3) (Figure 3) indicate that these bands are not related to the same dicarbonyl adduct. Moreover, the 2197 cm^{-1} band is produced after the others. These features show that these three absorptions are not correlated to each other and must be assigned to distinct types of dicarbonyl species.

Dicarbonyl species of low symmetry are known to exhibit two IR active CO stretching modes, one symmetric ($\nu_{CO_{sym}}$) and one antisymmetric ($\nu_{CO_{asym}}$), the latter usually producing the absorption band located at the lower frequency.[31a] The intensity ratio between the two components depends, among other factors, on the angle between the CO oscillators. This angle is usually found to be larger than 90°, leading to a higher intensity of the antisymmetric band.

Because no other absorption exhibiting a higher intensity is observed in the spectra, the three independent 2197, 2180, and

TABLE 1: Experimental and Calculated Frequencies of $Ni^{II}(CO)_2$ with Equivalent COs (Type A Dicarbonyl) for $ENi(NH_3)$[a]

dicarbonyl	freq	calcd	exptl
$(^{12}CO)_2$	ν_s	2206	2207
	ν_a	2180	2181−2180
$(^{13}CO)_2$	ν_s	2157	2156[b]
	ν_a	2131	2131[b]
$(^{12}CO)(^{13}CO)$	ν_s	2196	2196
	ν_a	2141	2142

[a] CO bond force constant, $F_{CO} = 19.430$ mdyn Å^{-1}; CO interaction force constant, $f_{CO-CO} = 0.232$ mdyn Å^{-1}. [b] Measured in a separate experiment with ^{13}CO

TABLE 2: Experimental and Calculated Frequencies of $Ni^{II}(CO)_2$ with Nonequivalent COs (Type B Dicarbonyl) for $ENi(NH_3)$

dicarbonyl	freq	calcd	exptl
$(^{12}CO)_2$	ν_s	2179	*b*
	ν_a	2108	2107
$(^{13}CO)_2$	ν_s	2130	2130[c]
	ν_a	2061	2060[c]
$(^{12}CO)_a(^{13}CO)_b$[d]	ν_s	2177	2176_{sh}[e]
	ν_a	2063	2062
$(^{12}CO)_b(^{13}CO)_a$[d]	ν_s	2139	*g*
	ν_a	2099	2100_{sh}[e]
$(^{12}CO)_e(^{13}CO)_e$[f]	ν_s	2161	
	ν_a	2077	

[a] CO bond force constants, $F_{CO_a} = 19.080$ mdyn Å^{-1} and $F_{CO_b} = 18.050$ mdyn Å^{-1}; subscripts a and b represent positions of nonequivalent CO oscillators. CO interaction force constant, $f_{CO-CO} = 0.340$ mdyn Å^{-1}. [b] Overlapped with the 2180 cm^{-1} band of type A dicarbonyl (Table 1). [c] Observed in a separated experiment with ^{13}CO. [d] Subscripts a and b represent the positions of nonequivalent CO oscillators. [e] Subscript sh indicates shoulder. [f] Subscript e represents equivalent CO oscillators of which the frequencies for $(^{12}CO)_2$ are observed at 2180 and 2107 cm^{-1}. [g] Overlapped with the 2142 cm^{-1} band.

2107 cm^{-1} bands are assigned to the $\nu_{CO_{asym}}$ antisymmetric mode of three different types of dicarbonyls, each of these bands being coupled with a weaker component at higher frequency corresponding to the $\nu_{CO_{sym}}$ mode.

2.2. Bands at 2207 and 2180 cm^{-1}: Type A Dicarbonyl with Equivalent COs. The weak component at 2207 cm^{-1}, which increases in intensity together with the 2180 and 2107 cm^{-1} components while the 2201 cm^{-1} band is progressively depleted (Figure 1B), appears to be related to one of these two antisymmetric bands. By considering its position, it could correspond to the high frequency $\nu_{CO_{sym}}$ mode coupled with the $\nu_{CO_{asym}}$ absorbing at 2180 cm^{-1}.

To verify whether these two components are coupled, calculations of the expected absorption frequencies of a corresponding mixed $^{12}CO-^{13}CO$ dicarbonyl species have been carried out by using the simplified Cotton−Kraihanzel harmonic force field approximation (C−K HFF), hereafter referred to as C−K,[32] and the calculated values have been compared to the experimental frequencies obtained by adsorbing the $^{12}CO-^{13}CO$ (50:50) mixture onto the sample (Figure 2 and Table 1).

As reported in Table 1, the substitution of one ^{12}CO by one ^{13}CO in the $(^{12}CO)_2$ dicarbonyl species with two equivalent oscillators absorbing at 2207 and 2181−2180 cm^{-1} produces a mixed species exhibiting bands at 2196 and 2141 cm^{-1}, and this accounts for the occurrence of the bands at 2196 and 2142 cm^{-1} (Figure 2, spectr a−c). Thus, the 2207 and the 2181−2180 cm^{-1} bands may be assigned to a $Ni^{II}{}_{3c}(CO)_2$ species with two equivalent COs.

2.3. Bands around 2180 and 2107 cm^{-1}: Type B Dicarbonyl with Nonequivalent COs. For the 2107 cm^{-1} band, no resolved weaker component coupled with this absorption and located at higher frequency is visible. However, when the 2181 cm^{-1} band increases in intensity, it undergoes a progressive broadening and a slight shift toward lower frequencies. Such a behavior could be partly related to the growth, on the low-frequency side, of an unresolved component corresponding to the $\nu_{CO_{sym}}$ mode coupled with the 2107 cm^{-1} one. In the case of the ENi(en) sample, the 2180 cm^{-1} component appears quite narrower while the band at 2105 cm^{-1} is significantly weaker in intensity than that observed for the $ENi(NH_3)$ sample at 2107 cm^{-1} (Figure 3).

To verify this hypothesis, calculations of the positions of the corresponding mixed $^{12}CO-^{13}CO$ dicarbonyls have been carried out by means of the C−K approximation, supposing the frequency of the $\nu_{CO_{sym}}$ component to be in the 2180−2177 cm^{-1} range and the $\nu_{CO_{asym}}$ one at 2107 cm^{-1}. A strong discrepancy between calculated and experimental values has been found when considering equivalent COs. In this case, mixed $^{12}CO-^{13}CO$ species are expected to absorb at 2161 and 2077 cm^{-1} (Table 2), whereas no band is present at these frequencies in the spectra reported in Figure 2. By contrast, as shown in Table 2, a satisfying agreement is obtained by assuming nonequivalent COs. The nonequivalence of the coupled oscillators is reflected by different CO force constants (corresponding to two different F_{CO} and F'_{CO} values in the C−K approximation).[33]

Indeed, in the spectra shown in Figure 2a−c, it is possible to recognize the absorptions expected at 2177 and 2063 cm^{-1} in the shoulder at 2176 cm^{-1} observed on the 2180 cm^{-1} band and in the 2062 cm^{-1} component, respectively. Considering the 2139 and 2099 cm^{-1} signals, the first one contributes to the intensity of the neighboring peak at 2142 cm^{-1}, while the second one appears as an unresolved component in the broad absorption around 2107 cm^{-1}.

The existence of a tricarbonyl species with equivalent COs, which is expected to exhibit two CO stretching bands,[31b] was also taken into consideration. The calculated frequencies of the mixed species did not correspond to the values of the new bands observed with the $^{12}CO-^{13}CO$ (50:50) mixture. Moreover, experiments performed with $^{12}CO-^{13}CO$ mixtures of different compositions (25:75 and 75:25), showed that the relative intensities of the mixed species did not vary with the composition of the $^{12}CO-^{13}CO$ mixture, which unambiguously demonstrates that no species other than the dicarbonyl ones were produced.

To provide a more quantitative basis for the interpretations of the various dicarbonyls observed, simulations of the observed absorption profiles based on the C−K frequency calculations and additional assumptions were attempted.[34]

Figure 4 displays the simulation results using θ_A and θ_B values of 140° and 100°, respectively, yielding a better overall agreement with the observed spectrum than with other significantly different values. While the simulated profile reproduces fairly well the observed isotopic pattern frequencies, the agreement is not quantitatively satisfactory regarding relative intensities and profiles. This is hardly surprising, given the large number of necessary approximations and the fact that the experimental profiles of individual bands are also often nonsymmetrical. Even if the present model is not perfect, it seems that all of the observed features can now be satisfactorily accounted for.

2.4. Origin of the Nonequivalence of the COs in Type B Dicarbonyl. To elucidate the origin of the nonequivalent character of the two CO oscillators, it can be emphasized that the 2107 cm^{-1} band exhibits a significant dependence on the

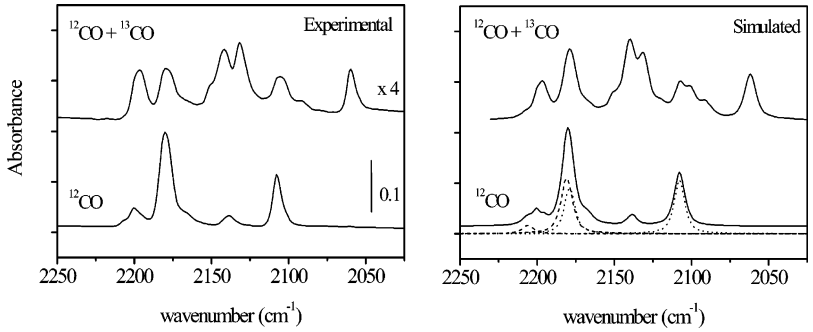

Figure 4. Simulated and experimental spectra of ^{12}CO and $^{12}CO-^{13}CO$ (50:50) mixture adsorbed at 77 K under a pressure of 60 Pa on $ENi(NH_3)$. The procedure for simulation is detailed in ref 34.

degree of dispersion of the Ni^{II}_{3c} ions on the support, because it is strongly reduced in intensity in the case of the ENi(en) sample, which contains a higher fraction of isolated Ni^{II}_{3c} ions (Figure 3, spectrum a).[22a] Such a dependence suggests that these dicarbonyls with nonequivalent CO are formed from Ni^{II}_{3c} with other Ni^{II} ions in their proximity.

The nonequivalence of CO oscillators has been shown for alkali (M^+) salts of $CpM'(CO)_3^-$, where M′ stands for a transition metal and $Cp = C_5H_5$, and of $(\eta^5\text{-}C_5H_5)Fe(CO)_2^-$ in THF solutions.[35,36] The nonequivalence of the CO oscillators is revealed by the bridging interaction of one of the CO with the alkali metal through the oxygen, giving rise to the lowering of the ν_{CO} frequency. The same effect was reported for ruthenium dinitrosyl complexes.[37]

Therefore, the observed nonequivalence of the CO oscillators in type B dicarbonyl (2179−2107 cm^{-1} bands) may be interpreted by the fact that one CO is coordinated in a bent way (by a bridging interaction of the oxygen atom of a CO) to another adjacent Ni^{II} ion located at the surface of a neighboring NiO particle (see part I in which the band at 2140 cm^{-1} was attributed to low-coordinated Ni^{II} sites at the surface of small NiO particles).[23]

This interpretation agrees with the lower frequencies of the stretching modes of type B dicarbonyl with nonequivalent COs (2179 (calculated), 2107 cm^{-1} (experimental)) in comparison with those of type A dicarbonyl with equivalent COs (2206, 2180 cm^{-1}) (see Tables 2 and 1, respectively). The number of Ni^{II} ions suitably located to permit such a bridging interaction is expected to decrease by increasing the dispersion of the surface centers on the support, which accounts for the lower intensity of the bands of type B dicarbonyl in the spectra of the ENi(en) sample.

At the highest CO pressure, bands due to types A and B do not increase in intensity, while the residual part of the monocarbonyl is transformed into another dicarbonyl through an isobestic point (inset of Figure 1C). This minor species (type C) is commented on in Supporting Information, section 1.

B. Quantum Chemical Calculations. In this section, calculations of the geometric parameters for the dicarbonyl Ni^{II} complexes are performed by using the $Si_5O_3^-$ silica cluster composed of $(SiO)(SiOSi)_2$ fragments, composed of one silanolate and two siloxane bridges, previously selected as the best candidate able to simulate the experimental results. In particular, it reproduced fairly well the short (1.75 Å) and long (2.02 Å) NiO distances found by EXAFS for the Ni^{II}_{3c} ion[22a] and the CO frequencies of the corresponding monocarbonyl Ni^{II}_{3c} complexes.[23] Then, the $[(Si_5O_3)Ni^{II}]^+$ cluster is embedded in silica rings existing at the surface of amorphous silica.

1. Modeling Silica with the $Si_5O_3^-$ Cluster: Dicarbonyl Ni^{II} Complexes. 1.1. Geometric Parameters and Frequency Calculations. No minimum in the potential energy surface corresponding to a dicarbonyl Ni^{II} complex tricoordinated to the silica clusters could be obtained; the structure evolved toward a dicoordinated Ni^{II}_{2c} complex. This indicates that the formation of the dicarbonyl complex occurs through a ligand displacement process in which one of the silica ligands is replaced by CO. To model the silica-like cluster that binds to the dicarbonyl Ni^{II} complex, two fragments are thus needed. The siloxane group located at the largest Ni−O distance was excluded.

The two COs can be in cis or trans position as previously mentioned by Rebenstorf and Larsson.[21] Three minima in the potential energy surface were found, corresponding to one cis and two trans configurations, a trans square planar-like and a trans distorted square planar configuration, referred to as trans square planar and trans distorted, respectively (Tables 3 and 4). Table 3 gathers the calculated geometric parameters found for these dicarbonyl complexes in the optimized configurations, using the above-mentioned silica cluster model.[27]

TABLE 3: Optimized Geometric Parameters for Dicarbonyl Ni^{II}_{2c} Complexes

	(SiO)(SiOSi) cluster geometry		
parameter	cis square planar	trans square planar	trans distorted
r(Ni−C) (Å)	1.775	1.879	1.894
	1.859	1.879	1.894
r(C−O)[a] (Å)	1.137	1.136	1.137
	1.138	1.136	1.137
r(Si···Si) (Å)	5.6	5.9	6.5
	5.6	6.3	6.2
	3.0[b]	3.1[b]	3.0[b]
∠CO−CO (deg)	90	168	147
∠O−Ni−O (deg)	111	165	164

[a] Calculated for free CO = 1.146 Å. [b] Si···Si distance in SiOSi.

TABLE 4: Calculated Frequencies for Dicarbonyl Ni^{II}_{2c} Complexes[a]

	(SiO)(SiOSi) cluster geometry		
parameter	cis square planar	trans square planar	trans distorted
calcd CO freq (cm^{-1})	2229, 2210	2240, 2209	2215 (2213)[b] {+9}; 2198 (2191)[b] {−13}
intensities of CO bands ($km \cdot mol^{-1}$)	335, 245	2, 147	26, 378

[a] Experimental frequencies (cm^{-1}) of type A dicarbonyl, $\nu_s = 2207$ {+6} and $\nu_a = 2181$ {-20}. [b] Calculated by setting the Si···Si distances at the values found in the monocarbonyl complex optimized from the bare Ni^{II}_{3c} ion. The figures in braces { } express the frequency shift with respect to the calculated monocarbonyl frequency (2204 cm^{-1}) for the (SiO)(SiOSi) clusters.

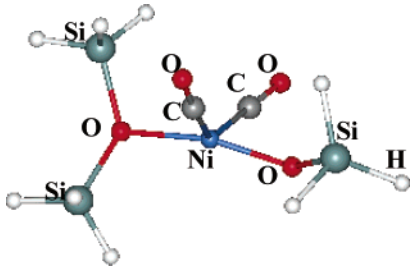

Figure 5. Optimized structure (B3LYP) of the dicarbonyl Ni^{II} complex bound to the (SiO)(SiOSi) clusters.

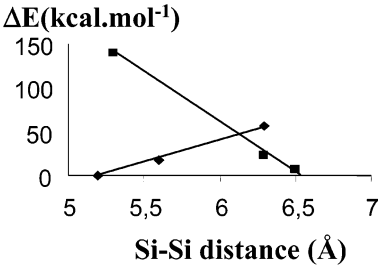

Figure 6. Energy minima of the dicarbonyls in the cis and trans distorted (type A) configurations (◆, cis; ■, trans) as a function of the Si···Si distances.

The C−O bond lengths are shorter than that of free CO, as already observed for the monocarbonyl complex.[23] The Si···Si distances exhibit shorter values in the cis (5.2 Å) than in the trans configuration (>6 Å) (except for the short Si···Si distance in the siloxane SiOSi bridge). The CO−CO angle stongly varies with the configuration.

The calculated CO frequencies are compared to the experimental values of the mono- and dicarbonyl complexes in Table 4. No negative frequencies are found, indicating that the calculated points are local minima. In the trans distorted configuration, the calculated CO frequencies fit better the experimental values than those in the other configurations. The dicarbonyl complexes in this configuration with the (SiO)(SiOSi) fragments are represented in Figure 5.

1.2. Tricarbonyl Ni^{II} Complex. The IR results show that the tricarbonyl complex does not form. It was not possible to reach a minimum in the potential energy surface for the tricarbonyl Ni^{II} complex with a nickel dicoordinated to the cluster; the structure evolves toward a dicarbonyl complex. Even if a ligand displacement of the silica surface is assumed by adding a third CO molecule, the formation of the tricarbonyl Ni^{II} complex monocoordinated to silica is not favored because the above reaction is found to be endothermic (+19.2 kcal·mol^{-1}).

1.3. Discussion. The results concerning type A dicarbonyl with equivalent COs are confronted with the modeling calculations. The different configurations (cis and trans) calculated for type A dicarbonyl are then commented on.

1.3.1. Assignment of the Trans Distorted Configuration to Dicarbonyls with Equivalent COs (Type A Dicarbonyl). Among the three geometric configurations (cis, trans square planar, and trans distorted), only the dicarbonyl complex in the distorted trans geometry may be assigned to type A dicarbonyl because the calculated CO frequencies, CO−CO angle, and intensities of the bands give the best fit with the experimental results. In this configuration, the calculated (DFT) CO−CO angle (∼147°) (Table 3) is in good agreement with the value of 140° found with the C−K approximation. The cis configuration, although slightly more stable than the trans distorted one by −7 kcal·mol^{-1}, must be discarded because the calculated frequencies do not fit the experimental ones.

It must be noted that the observation of a major type of dicarbonyl (type A) despite the fact that several configurations are predicted by calculations confirms that Ni is in a single environment as previously reported.[22a]

1.3.2. Stability of the Dicarbonyl Configuration as a Function of the Silica Constraints. As mentioned above, the three optimized configurations (cis, trans square planar, and trans distorted) are strongly related to the CO−CO angle and the Si···Si distances. Figure 6 shows the energies of the optimized configurations with the (SiO)(SiOSi) cluster as a function of the Si···Si distance. The cis configuration is the most stable for Si···Si distances <6.1 Å, whereas the trans distorted configuration (type A dicarbonyl) becomes the most stable for Si···Si distances >6.1 Å. The fact that the experimental dicarbonyl (type A) is the predominant species and energetically less stable (by 7 kcal·mol^{-1}) than the cis dicarbonyl suggests that the Si···Si distance is >6.1 Å and that the activated silica is rigid enough because it cannot relax to generate a cis dicarbonyl.

1.3.3. Thermodynamics of the Carbonyl Ni^{II} Complexes. IR experiments showed that dicarbonyls form at the same time as monocarbonyls at very low CO pressure (Figure 1A) and then grow at the expense of monocarbonyls at higher CO pressure (Figure 2B). This can be explained by considering the calculated CO binding energies of the formation of the mono- and Ni^{II} dicarbonyls with equivalent COs as expressed in the Supporting Information, section 2.

2. Modeling Silica with Cycles (nT). 2.1. Choice of the Convenient Cycle. The preceding $[(SiO)(SiOSi)_2Ni]^+$ cluster allows us to model the interactions of Ni^{II}_{3c} with CO, although it does not take into account the complexity of the silica surface. This is the reason that we can embed now this fragment in silica cycles (rings) that constitute the surface of annealed silica. The surface of silica is constituted by *n*-fold rings, which can be planar or puckered.[38,39] We will use hereafter the terminology accepted in zeolite chemistry in which the size of the ring is referred to as the number of T atoms (T = Si or Al). Therefore *n*T represents here the number of Si atoms.

We will consider *n*T cycles of increasing size, taking into consideration that the model Ni−*n*T cycle must obey the same criteria as those obtained by using the fragment $[(SiO)(SiOSi)_2Ni]^+$. These criteria are 3-fold Ni coordination, mean ratio of short/long Ni−O bond length = 2/1,[22a] overall charge of the site = +1, absence of a SiOH bound to Ni^{II}, formation of one single monocarbonyl Ni complex,[23] formation of a single dicarbonyl Ni complex with equivalent COs (type A), and finally Si···Si distances of >6.1 Å (this work).

The schemes shown in Scheme 1 represent some of the possible configurations of the Ni^{II} ion in 3T−6T cycles. These cycles contain a terminal SiO^- and at least two siloxane bridges, which gives rise to a 1+ charge for the Ni complex. However, the other criteria above-mentioned are not fulfilled. Thus, for the 3T−5T series, the Si···Si distances are <6.5 Å. The Ni complex in the 3T cycle configuration is in 3-fold coordination, whereas the Ni complex in 4T and 5T cycles is in 4-fold coordination. DFT calculations give also rise to a 4-fold Ni coordination for the 6T and 7T cycles (7T scheme not represented for the sake of brevity). Therefore, all of these configurations have to be discarded.

Larger cycles such as 8T and 9T cycles allow the Ni^{II} ion to be again stabilized in 3-fold coordination because the non-coordinated oxygen atoms are far enough from nickel. However, the free optimization of the Ni 8T and 9T cycles leads to one short and two long Ni−O distances, as previously observed with

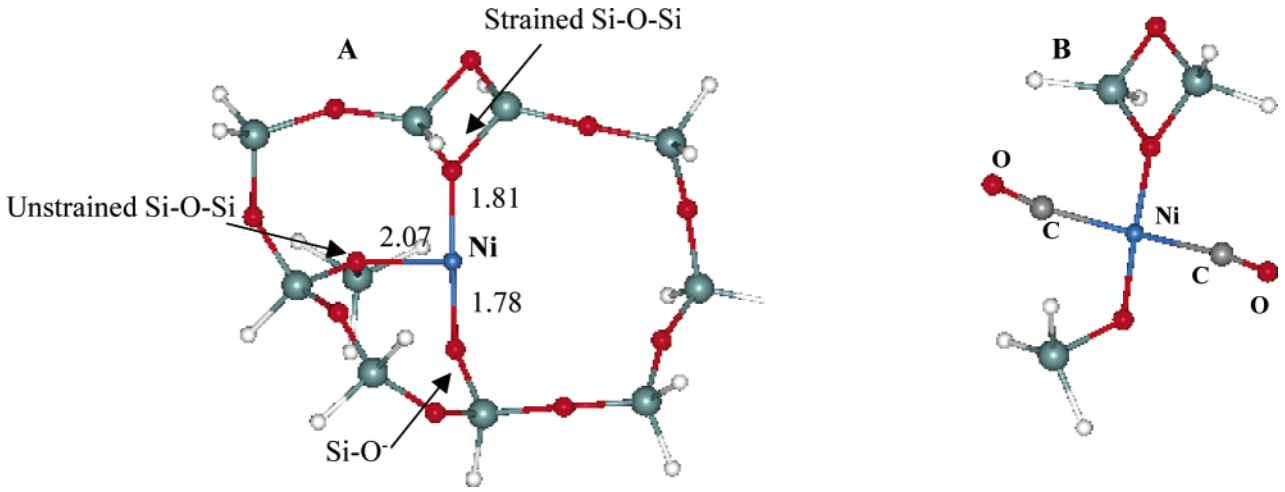

Figure 7. Optimized structure (A) of the Ni^{II}_{3c} ion in a 9T ring with an adjacent 2T ring and (B) dicarbonyl formed with (SiO)(SiOSi) fragments cut from the Ni 9T−2T cycle.

SCHEME 1: Possible Configurations of the Ni^{II} Ion in 3T−6T Cycles Representing the Surface of Amorphous Silica

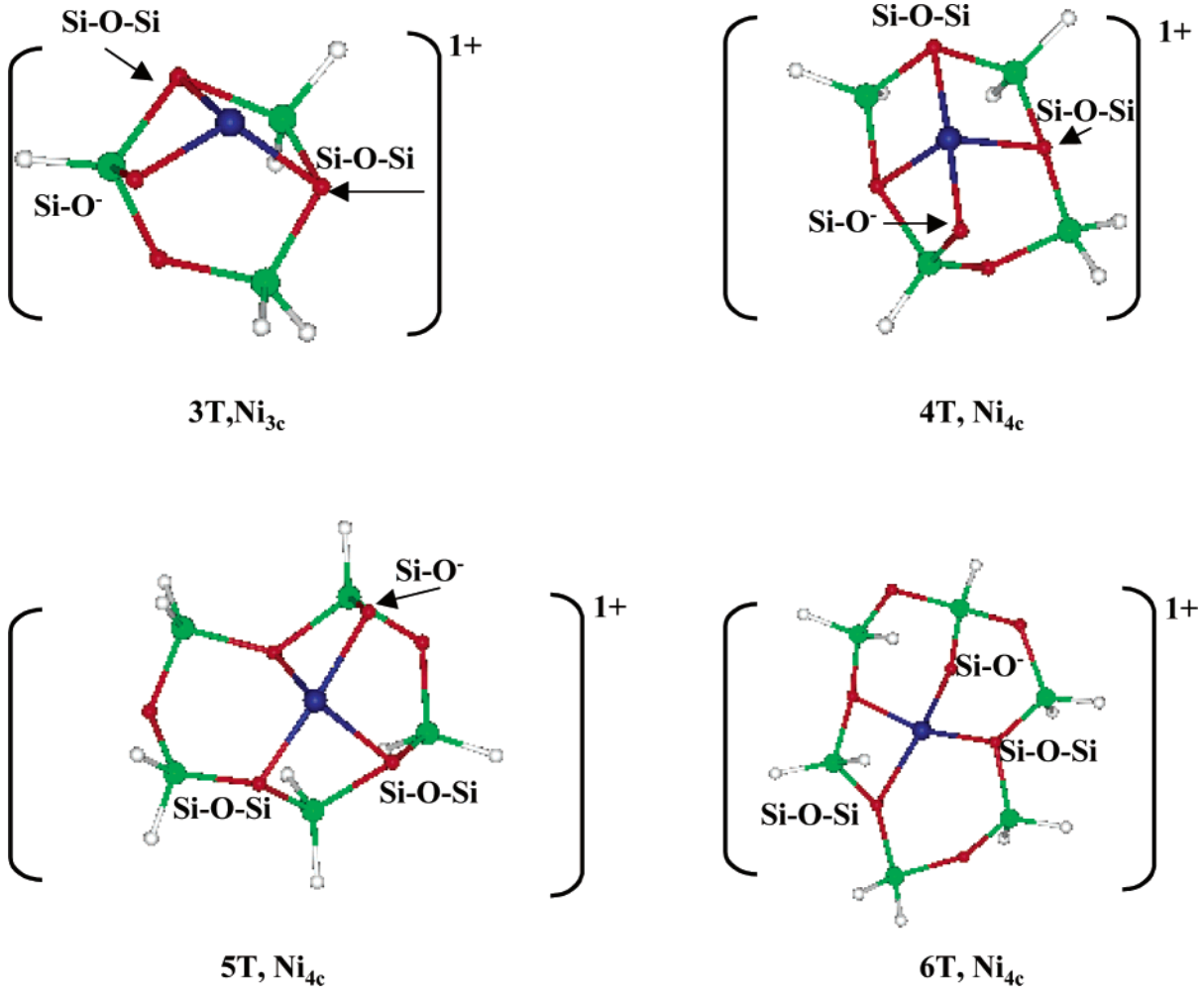

the $Si_5O_3^-$ fragment,[23] which disagrees with the EXAFS results.[22a] This is the reason that a constraint has to be added to obtain two short Ni−O distances. The best way is to introduce a strained siloxane by including an adjacent 2T cycle. Figure 7 represents the optimized Ni in a 9T cycle with an adjacent 2T cycle (referred to as 9T−2T).[40] The optimization of the Ni 9T−2T cycle forces the SiOSi angle to attain a value (93°) smaller than that observed for silica (150°), and this in turn favors a shorter Ni−O bond length (1.81 Å). Strained siloxanes with a SiOSi angle near 90° are reported by Bunker et al.[41] and Nedelec and Hench,[42] whereas the mean value of an unstrained SiOSi angle in silica is found to be 144° and 153°, respectively.[41,42]

Thus, the best configuration corresponds to a Ni^{II} ion tricoordinated in an 8T or 9T cycle with a neighboring 2T ring. To check the validity of this model, fragments were cut from the Ni 9T−2T cycle as shown in Figure 7 and the dicarbonyl Ni complex with equivalent COs was optimized.[44] The calcu-

lated CO frequencies (2204 and 2180 cm^{-1}) reproduce well the experimental values (2207 and 2181 cm^{-1}).

2.2. Discussion. One can wonder whether the 9T−2T cycle model is realistic. In short, what is the probability to find on the surface of amorphous silica large cycles such as 8T or 9T close to very small cycles (2T)? There seems to be a general agreement that 5T and 6T rings are the most frequenly found, both in the bulk and on the surface, as observed experimentally[45] and obtained from random models,[46−48] cluster calculations,[42] and cristobalite-derived models.[49] Larger rings such as 8T and 9T are also found.[46,47,50] The smaller 2T and 3T rings, which are less common, are produced on annealed silica by condensation of SiOH groups.[41,51,52] Feuston and Garofalini report that the silica surface is more enriched in 2T and 3T rings than the bulk.[46a] The proximity of small 2T rings to larger rings such as 7T was reported by Ceresoli et al.[50] These data suggest that the model proposed to accommodate the Ni^{II} ion in 3-fold coordination, shown in Figure 7, is realistic. It is important to note that the amount of Ni^{II}_{3c} ions (0.7 Ni/nm^2) is on the order of the 2T rings surface concentration as estimated from calculations[46,48] (0.13−0.75 2T rings/nm^2) and experimentally[53] (0.2−0.4 /nm^2).

The role played by the presence of small 2T or 3T rings in the adsorption of $[Ni(en)_2(H_2O)_2]^{2+}$ on silica has also been emphasized in a recent work from our laboratory.[54] It is suggested that the interaction of this complex with silica involves the formation of H bonds between the NH_2 ligands of ethanediamine and oxygen of strained siloxanes arising from 3T rings.

In this work, we have shown that Ni^{II}_{3c} sites are homogeneously distributed in 8T or larger silica rings and bound to one SiO^-, one free siloxane, and one strained siloxane that belongs to a 2T ring. It would be interesting to relate these results to the deposition of Ni on silica, that is, the adsorption of the Ni(en) complex on the silica surface in basic medium. The stability of the 2T rings during deposition of the Ni complex is a key problem. The understanding of the combined presence of the large (8T or 9T) rings together with the adjacent strained siloxane in the accommodation of Ni at the solid−solution interface represents a future challenge.

Conclusion

In this work, we use both the Ni^{II} ion and the CO molecule as successive probes of the local structure and reactivity of the silica surface. CO acts not as a chemical reactant but as a molecular probe of the coordination vacancies of the grafted Ni^{II}_{3c} ion under conditions (adsorption at 77 K) that keep the metal oxidation state constant. The theoretical models representing Ni^{II}_{3c} grafted onto silica are then tested to see whether the experimental data can be reproduced.

The reactivity of the Ni^{II}_{3c} ions toward CO is tested for two samples, $ENi(NH_3)$ and ENi(en) (2 wt % Ni) with different surface dispersion of nickel. The complexity of the annealed silica surface is observed through the experimental IR study that shows the formation of one type of monocarbonyl and two types of dicarbonyl Ni complexes. The existence of one major type of dicarbonyl confirms that Ni is mainly in a single type of environment.[22a] From comparison between experimental data (CO IR frequencies) and theoretical models, it is possible to significantly improve our understanding of the environment of the Ni^{II}_{3c} ion. Indeed, increasing the CO pressure and thus forming dicarbonyl complexes allow us to extend the information to the second coordination sphere of the Ni^{II} ion and thus to Si atoms, whereas for the monocarbonyl complex reported earlier,[23] the first oxygen nearest neighbors only were concerned.

The approach using small fragments is refined to take into account the complexity of the silica surface. By embedding the selected silica fragment, $[(Si_5O_3)Ni^{II}]^+$, in silica rings present at the surface of silica, we try to bridge the reality gap existing between a model and the real system. We show that the Ni^{II} ions are homogeneously distributed in 8T or larger silica rings and bound to one silanolate SiO^-, one free siloxane SiOSi, and one strained siloxane that belongs to an adjacent 2T ring to form the Ni^{II}_{3c} grafted ion. Using this single model, we show that the entire set of experimental results (mainly NiO distances and CO IR frequencies) can satisfactorily be accounted for.

Acknowledgment. The authors warmly thank Dr. C. Lepetit for judicious advice for the modeling study and Profs. J. F. Lambert and P. Chaquin for helpful discussions. G. Martra acknowledges the Italian Consiglio Nazionale delle Ricerche for financial support (CNR-NATO Fellowship 215.27/03).

Supporting Information Available: Section 1 discussing bands at ∼2207 and 2197 cm^{-1} (type C dicarbonyl) and section 2 discussing thermodynamics of the carbonyl Ni^{II} complexes. This material is available free of charge via the Internet at http://pubs.acs.org.

References and Notes

(1) Browne, V. M.; Fox, S. G.; Hollins, P. *Catal. Today* **1991**, *9*, 1−14.
(2) Hollins, P. *Surf. Sci. Rep*. **1992**, *16*, 51−94.
(3) (a) Knözinger, H. In *Handbook of Heterogeneous Catalysis*; Ertl, G., Knözinger, H., Weitkamp, J., Eds.; Wiley-VCH: Weinheim, Germany, 1997; Vol. 2, pp 707−732. (b) Coluccia, S.; Marchese, L.; Martra, G. *Microporous Mesoporous Mater*. **1999**, *30*, 43−56.
(4) Gates, B. C. *Chem. Rev*. **1995**, *95*, 511−522.
(5) Solymosi, F.; Pasztor, M. *J. Phys. Chem*. **1986**, *90*, 5312−5317. Solymosi, F.; Knözinger, H. *J. Chem. Soc., Faraday Trans. 1* **1990**, *86*, 389−395.
(6) Primet, M. *J. Chem. Soc., Faraday Trans. 1* **1978**, *74*, 2570−2580.
(7) Gelin, P.; Coudurier, G.; Ben Taarit, Y.; Naccache, C. *J. Catal*. **1981**, *70*, 32−40.
(8) (a) Zecchina, A.; Bordiga, S.; Salvalaggio, M.; Spoto, G.; Scarano, D.; Lamberti, C. *J. Catal*. **1998**, *173*, 540−542. (b) Lamberti, C.; Palomino, G. T.; Bordiga, S.; Berlier, G.; D'Acapito, F.; Zecchina, A. *Angew. Chem., Int Ed*. **2000**, *39*, 2138−2141.
(9) Louis, C.; Che, M. *J. Phys. Chem*. **1987**, *91*, 2875−2883.
(10) Guglielminotti, E.; Giamello, E. *J. Chem. Soc., Faraday Trans. 1* **1985**, *81*, 2307−2322. Zaki, M. I.; Vielhaber, B.; Knözinger, H. *J. Phys. Chem*. **1986**, *90*, 3176−3183.
(11) Knözinger, H.; Zhao, Y.; Tesche, B.; Barth, R.; Epstein, R.; Gates, B. C.; Scott, J. P. *Faraday Discuss*. **1981**, *72*, 53−71.
(12) Zanderighi, G. M.; Dossi, C.; Ugo, R.; Psaro, R.; Tholier, A.; Choplin, A.; D'Ornelas, L.; Basset, J. M. *Organomet. Chem*. **1985**, *296*, 127−146.
(13) Yokomizo, G. H.; Louis, C.; Bell, A. T. *J. Catal*. **1989**, *120*, 1−14.
(14) Guglielminotti, E. *Langmuir* **1986**, *2*, 812−820.
(15) Solymosi, F.; Erdöhelyi, A.; Kocsis, M. *J. Chem. Soc., Faraday Trans. 1* **1981**, *77*, 1003−1010.
(16) Davydov, A. A.; Bell, A. T. *J. Catal*. **1977**, *49*, 332−344.
(17) Yamasaki, H.; Kobori, Y.; Naito, S.; Onishi, T.; Tamaru, K. *J. Chem. Soc., Faraday Trans. 1* **1981**, *77*, 2913−2925.
(18) Goodwin, J. G., Jr.; Naccache, C. *J. Catal*. **1980**, *64*, 482−486.
(19) Hadjiivanov, K.; Lavalley, J. C.; Lamotte, J.; Maugé, F.; Saint-Just, J.; Che, M. *J. Catal*. **1998**, *176*, 415−425.
(20) (a) Bonneviot, L.; Olivier, D.; Che, M. *J. Mol. Catal* **1983**, *21*, 415−430. (b) Lepetit, C.; Kermarec, M.; Olivier, D. *J. Mol. Catal*. **1989**, *51*, 73−93.
(21) Rebenstorf, B.; Larsson, R. (a) *Z. Anorg. Allg. Chem*. **1979**, *453*, 139−152. (b) *Z. Phys. Chem. Neue Folge* **1982**, *133*, 119−127.
(22) (a) Carriat, J. Y.; Che, M.; Kermarec, M.; Verdaguer, M.; Michalowicz, A. *J. Am. Chem. Soc*. **1998**, *120*, 2059−2070. (b) Garrot, J. M.; Lepetit, C.; Che, M.; Chaquin, P. *J. Phys. Chem. A* **2001**, *105*, 9445−9453.
(23) Costa, D.; Martra, G.; Che, M.; Manceron, L.; Kermarec, M. *J. Am. Chem. Soc*. **2002**, *124*, 7210−7217.
(24) Frisch, M. J.; Trucks, G. W.; Schlegel, H. B.; Gill, P. M. W.; Johnson, B. G.; Robb, M. A.; Cheeseman, J. R.; Keith, T.; Petersson, G. A.; Montgomery, J. A.; Raghavachari, K.; Al-Laham, M. A.; Zakrzewski, V. G.; Ortiz, J. V.; Foresman, J. B.; Cioslowski, J.; Stefanov, B. B.; Nanayakkara, A.; Challacombe, M.; Peng, C. Y.; Ayala, P. Y.; Chen, W.; Wong, M. W.; Andres, J. L.; Replogle, E. S.; Gomperts, R.; Martin, R. L.;

Fox, D. J.; Binkley, J. S.; Defrees, D. J.; Baker, J.; Stewart, J. P.; Head-Gordon, M.; Gonzalez, C.; Pople, J. A. *Gaussian 94*, revision B.1; Gaussian, Inc.: Pittsburgh, PA, 1995.

(25) Becke, A. D. *J. Chem. Phys*. **1993**, *98*, 5648. Lee, C.; Yang, W.; Parr, R. G. *Phys. Rev. B* **1988**, *37*, 785−789.

(26) Gotbout, N.; Salahub, D. R.; Andselm, J.; Wimmer, E. *Can. J. Chem*. **1992**, *70*, 560−571.

(27) The silica surface was modeled using first simple ligands $[(OH)(H_2O)]^-$ and then fragments of silica $[(SiO)(SiOSi)]^-$, as mentioned in the first paper (part 1, ref 23). Two configurations may be expected for the dicarbonyl Ni^{II} complexes: a cis and a trans configurations. When the silica surface is modeled using simple ligands $[(OH)(H_2O)]^-$, two minima in energy are found after full optimization. For the cis complex, the CO−CO and ONiO angles are close to 90 °C, and the two CO are in the ONiO plane. In contrast, for the trans complex, the CO−CO and ONiO angles are close to 170° and the CO oscillators are in a plane perpendicular to the ONiO plane. This result suggests that (i) the CO−CO angle depends on the ONiO angle, that is, on the geometrical constraints imposed by the silica support, that is, on the Si···Si distances, and (ii) other energy minima depending on the silica constraints may exist between those minima. With the silica fragments $[(SiO)(SiOSi)]^-$, the cis and the trans carbonyls fully optimized exhibit Si···Si distances varying from 5.2 (cis) to 6.3 Å (trans). However, the experimental CO frequencies corresponding to type A dicarbonyl cannot be reproduced. This is the reason that we have set the CO−CO angle at the value deduced from the calculated IR intensities in the C−K approximation (140°), while relaxing the other geometrical parameters. The Si···Si distance was then fixed at the distance found for the optimized complex, that is, 6.5 and 6.2 Å for $[(SiO)(SiOSi)]^-$, while the other parameters were allowed to relax. In these conditions, the CO−CO angle stabilized at an angle of 147°, very close to the experimental value (140°). The absence of any negative frequency confirmed the existence of a local minimum of energy. The calculated CO frequencies fit satisfactorily the experimental values (Table 4).

(28) Ghiotti, G.; Garrone, E.; Morterra, C.; Boccuzzi, F. *J. Phys. Chem*. **1979**, *83*, 2863−2869. Beebe, T. P.; Gelin, P.; Yates, J. T. *Surf. Sci*. **1984**, *148*, 526−550.

(29) Bor, G. J. *Organomet. Chem*. **1967**, *10*, 343−359. Haas, J. H.; Sheline, R. K. *J. Chem. Phys.* **1967**, *10*, 2996−3021. Darling, J. H.; Ogden, J. S. *J. Chem. Soc., Dalton Trans.* **1972**, 2496−2503.

(30) Zecchina, A.; Spoto, G.; Ghiotti, G.; Garrone, E. *J. Mol. Catal*. **1994**, *86*, 423−446. Spoto, G.; Zecchina, A.; Bordiga, S.; Ricchiardi, G.; Martra, G. *Appl. Catal. B* **1994**, *3*, 151−172.

(31) Braterman, P. S. In *Metal Carbonyl Spectra in Organometallic Chemistry*; Maitlis, P. M., Stone, F. G. A., West, R., Eds.; Academic Press: London, 1975; (a) p 43; (b) p 44.

(32) Cotton, F. A.; Kraihanzel, C. S. *J. Am. Chem. Soc*. **1962**, *84*, 4432−4438. Cotton, F. A.; Kraihanzel, C. S. *Inorg. Chem*. **1963**, *2*, 533−540.

(33) In such a case, when a statistical isotopic exchange of half of the CO oscillators occurs, two different types of mixed dicarbonyls are formed. Each mixed species produces two CO stretching bands, and then four additional signals are expected upon adsorbing a $^{12}CO-^{13}CO$ mixture. If the CO are nonequivalent, the force field is underdetermined with one degree of freedom, using the isotopically pure species only. There are three unknowns (F_{CO}, F'_{CO}, and one f_{CO-CO}) for two frequencies for each isotopic species. Hence, the force field parameters have to be numerically adjusted to fit, at the best, the experimental frequencies for all isotopic species, including the isotopically mixed species. Table 2 displays the calculated and experimental frequency values.

(34) (1) In isotopic mixtures, the weights of the different isotopic counterparts of the same species are supposed to follow a statistical distribution. (2) Spectral line shapes are restricted to Voigt profiles (combination of Gaussian and Lorentzian profiles). (3) For the dicarbonyl species, both carbonyl stretching absorption bandwidths are supposed to be identical within each species. Also, their intensity ratios are calculated in the zero-order bond-dipole approximation, in which the contributions of each CO group to the total dipole moment derivative are supposed to be vectorially additive. (4) For type B dicarbonyls with nonequivalent CO, the bond dipole derivatives of each CO group are supposed to be identical. This hypothesis permits us to decrease the number of parameters. (5) For species C, in the absence of a clear indication concerning the behavior of their absorption in the $^{12}CO-^{13}CO$ mixtures, only those observed with either ^{12}CO or ^{13}CO are taken into account. In a first step, the choice of the values of the bond angles θ_A and θ_B between the carbonyl groups in the dicarbonyl species will determine the relative intensities of the carbonyl stretching vibrations within each pair, following the formula $I_{sym}/I_{asym} = (1 + \cos\theta)/(1 - \cos\theta)$. In a second step, the relative intensities *between different species* and the band profile are optimized to fit the observed spectrum with either ^{12}CO or ^{13}CO only. Finally, using the same parameters, the total absorption spectrum for the $^{12}CO-^{13}CO$ isotopic mixture is calculated and compared to the experimental one. When the agreement is poor, other values of θ_A and θ_B are selected, and the procedure repeated again. If a good agreement is obtained, it indicates that the model is self-consistent.

(35) Darensbourg, M. Y.; Jimenez, P.; Sackett, J. R.; Hanckel, J. M.; Kump, R. L. *J. Am. Chem. Soc*. **1982**, *104*, 1521−1530. Darensbourg, M. Y. In *Progress in Inorganic Chemistry*; Lippard, S. J., Ed.; Wiley and Sons: New York, 1985; Vol. 33, pp 221−244.

(36) Pannell, K. H.; Jackson, D. *J. Am. Chem. Soc*. **1976**, *98*, 4443−4446.

(37) Pierpont, C. G.; Van Derveer, D. G.; Durland, W.; Eisemberg, R. *J. Am. Chem. Soc*. **1970**, *92*, 4760−4762.

(38) Maniar, P. D.; Navrotsky, A. *J. Non-Cryst. Solids* **1990**, *120*, 20−25.

(39) Galeener, F. L. *J. Non-Cryst. Solids* **1982**, *49*, 53−62.

(40) The optimization of the 9T cycle was performed as follows: the three Ni−O bond lengths were kept fixed at the EXAFS values, and all other parameters were let free to relax; then, the Ni atom was relaxed, whereas all other atoms were fixed.

(41) Bunker, B. C.; Haaland, T. M.; Michalske, T. A.; Smith, W. L. *Surf. Sci*. **1989**, *222*, 95−118.

(42) Nedelec, J. M.; Hench, L. L. *J. Non-Cryst. Solids* **1999**, *255*, 163−170.

(43) Bell, J. R.; Dean, P. *Philos. Mag*. **1972**, *25*, 1381−1398.

(44) A $[(SiO)(Si_2O)_2Ni]^+$ cluster was cut from the optimized 9T−2T cycle. The equivalent dicarbonyl formed with this cluster was optimized in the trans distorted geometry; during this optimization, the Si atoms were kept fixed.

(45) (a) Cooper, A. R. In *Proceedings of Conference on Boron in Glass and Glass Ceramics, Alfred University*; Pye, L. D., Frechette, V. D.; Kreidl, N. J., Eds.; Plenum Press: New York, 1978; p 167. (b) Gladden, L. F.; Vignaux, M.; Chiananussati, P.; Griffiths, R. W.; Jackson, S. D.; Jones, J. R.; Sharrat, A. P.; Robertson, F. J.; Webb, G.; Chieux, P.; Hannon, A. C. *J. Non-Cryst. Solids* **1992**, *139*, 47−59.

(46) (a) Feuston, B. P.; Garofalini, S. H. *J. Chem. Phys*. **1989**, *91*, 564−570. (b) Garofalini, S. H. *J. Non-Cryst. Solids* **1990**, *120*, 1−12.

(47) Guttman, L.; Rahman, M. *Phys. Rev. B* **1988**, *37*, 2657−2668.

(48) Mischler, C.; Kob, W.; Binder, K. *Comput. Phys. Commun*. **2002**, *147*, 222−225.

(49) Brinker, C. J.; Broow, R. K.; Tallant, D. R.; Kirkpatrick, R. J. *J. Non-Cryst. Solids* **1990**, *120*, 26−33.

(50) Ceresoli, D.; Bernasconi, M.; Ialori, S.; Parinello, M.; Tosatti, E. *Phys. Rev. Lett.* **2000**, *84*, 3887−3890.

(51) Morrow, B. A.; Cody, J. A. *J. Phys. Chem*. **1976**, *80*, 1998−2004.

(52) Michalske, T. A.; Bunker, B. C. *J. Appl. Phys.* **1984**, *56*, 2686−2693.

(53) Grabbe, A.; Michalske, T. A.; Smith, W. L. *J. Phys. Chem*. **1995**, *99*, 4648−4654.

(54) Boujday, S.; Lambert, J.-F.; Che, M. *J. Phys. Chem. B* **2003**, *107*, 651−654.